Energetics and Structure of Complexes of Al^+ with Small Organic Molecules in the Gas Phase

F. Bouchard,[§] V. Brenner,[†,‡] C. Carra,[†,||] J. W. Hepburn,[§] G. K. Koyanagi,[§] T. B. McMahon,*[,§] G. Ohanessian,[†] and M. Peschke[§]

Department of Chemistry, University of Waterloo, Waterloo, Ontario, Canada N2L 3G1, Département de Chimie, Laboratoire des Méchanismes Réactionnels (URA 1307 CNRS), Ecole Polytechnique, 91128 Palaiseau Cedex, France, Institute de Chimie Physique, Universite de Fribourg, Perolles, Fribourg CH-1700, Switzerland, and Laboratoire de Chimie Theorique, DSM/DRECAM/SPAM, CE-CEA Saclay, 91191 Gif-sur-Yvette, France

Received: January 28, 1997; In Final Form: June 6, 1997[⊗]

A new experimental apparatus is described which permits the determination of binding energetics for metal−ligand complexes. This technique mates laser ablation for the generation of atomic metal ions with the environment of a high-pressure ion source which leads to rapid termolecular stabilization of metal ion-ligand complexes containing one or more ligands. The time resolved capability of the detection system allows equilibrium to be studied quantitatively for binding energies in the range of 5−30 kcal mol^{-1}. Such measurements of the absolute binding energy of formaldehyde to Al^+ combined with existing bimolecular Al^+ exchange equilibrium data leads to an absolute Al^+ affinity scale. For two ligand complexes an extensive *ab initio* search of the potential energy surfaces shows that the experimentally observed species involving CH_3CN and $(CH_3)_2O$ involve simple ligand complexation with an acute L-Al−L bond angle (L = ligand) rather than hydrogen bonded or inserted structures. In one instance a third ligand complexation has been experimentally investigated likely leading to a species of pyramidal geometry.

Introduction

The study of the energetics of complexes of metal cations with small organic and inorganic molecules has been an area of intense interest over the past several years. There have been many techniques used to investigate such species ranging from bracketing experiments,[1] photodissociation,[2] threshold-collision-induced dissociation (CID),[3] rate of infrared radiative cooling,[4] and equilibrium measurements.[5] The techniques potentially able to provide the most accurate determinations of binding energetics are the threshold CID and equilibrium measurements. The former has been exploited extensively, largely by Armentrout and co-workers, to elucidate the bonding in single- and multiligand complexes of metal ions.[6] This technique, while versatile, frequently requires the use of auxiliary data to transform the experimental threshold into a bond energy. When the species involved are small, the threshold determination usually provides an accurate measure of the bond dissociation energy. However, as the size and molecular complexity increase, the thermal energy of the parent ion can participate in the bond breakage and it is therefore important to have an accurate assessment of this thermal energy to properly convert the experimentally determined threshold to a bond energy. In order to do this a knowledge of the vibrational frequencies of the ion in question is required and such data are typically available only from high level quantum chemical calculations. In addition, these measurements are carried out on an experimental time scale, which may be short compared to the unimolecular dissociation lifetime of decomposing ions with near threshold energies. As a result it is necessary to carry out RRKM analysis of the dissociation which also requires accurate structural and vibrational data for the ion of interest. For this reason, bond energy determinations by threshold techniques for metal ion complexes of significant size might not be regarded as completely experimental quantities. Due to the difficulty in performing calculations on such species, this imposes some limitations on the applicability of the method.

Equilibrium measurements, such as those described by Bowers *et al.*,[7] are inherently more satisfactory because they provide thermochemical data based completely on experiment. This method involves deceleration of a metal ion beam from a magnetic sector spectrometer into a drift cell containing a known pressure of substrate to which the metal ion can bind. A sufficient number of collisions can occur that thermodynamic equilibrium may be assumed to be established. From a series of equilibrium measurements over a sufficiently large temperature range the values of $\Delta H°$ and $\Delta S°$ for the equilibrium may be obtained. Such experiments have been carried out for several transition metal ions clustering onto rare gases, dihydrogen, and small alkanes. In the few cases where comparison can be made, good agreement is obtained between the data derived from the equilibrium method and those from threshold CID measurements.

Following the emergence of experimental determinations of complexation energies, *ab initio* calculations have been carried out on complexes of metal ions with atoms and small molecules, prominently by Bauschlicher *et al.*[8] Such calculations have only relatively recently been possible with the advent of powerful computers because a reliable description of such complexes requires the use of extended basis sets and highly correlated wave functions. These calculations provide a detailed understanding of the electronic structure of metal−ion complexes, which can explain trends in binding energies of a series of metals to a given ligand. Also, trends in sequential binding energies of successive identical ligands to a given metal can be understood. It can be expected that such calculations will

[§] University of Waterloo.
[†] Ecole Polytechnique.
[||] Universite de Fribourg.
[‡] DSM/DRECAM/SPAM.
[⊗] Abstract published in *Advance ACS Abstracts,* August 1, 1997.

S1089-5639(97)00346-0 CCC: $14.00

become more common in the near future due to the development of density functional methods,[9] which have already been shown to be of an accuracy comparable to that of *ab initio* wavefunctions at much lower computational demand. In addition, unlike experimental methods, the quantum chemical calculations provide details of the molecular structure and vibrational frequencies of the complexes concerned. In this last respect they serve as an excellent complement to experimental measurements.

There have been relatively few experimental studies of the energetics of interaction of metal ions with more complex organic ligands.[3−5] The technique that will be described in the present article is inherently well suited to such studies. An ideal benchmark to assess the facility of this method might be found in the complexation of Al^+ with various small organic molecules. Using conventional ICR techniques Staley *et al.*[10] and Gal *et al.*[11] have derived a scale of relative binding free energies for small molecules to Al^+ on the basis of a series of bimolecular Al^+ transfer equilibria. Since only bimolecular Al^+ transfer reactions can be examined under these low-pressure ICR conditions, only the energetics associated with the transfer of Al^+ may be obtained. This is in contrast to the higher pressure experiment of Bowers *et al.*[7], and that to be described herein, where direct clustering equilibria may be examined and hence absolute binding energetics derived. In principle, a single direct-clustering measurement for the energetics of binding of Al^+ to any one of the molecules in the Staley−Gal relative scale would allow that scale to be converted to one of absolute binding energetics. *Ab initio* calculations exist already in the literature on a number of Al^+ complexes at a reliable level of theory,[12−15] which allow comparison with the resultant absolute experimental scale.

In the present work experiments are described which yield an absolute binding energy for Al^+ to one of the molecules in the Staley−Gal scale, formaldehyde, and allow the construction of an absolute Al^+ binding energy table. In addition, experiments are described that allow the determination of the energetics of association of a second ligand molecule to the Al^+ center. *Ab initio* calculations have been carried out on some of these complexes which generally show good agreement with experimental data for *both* the enthalpies and entropies of association. As well, in one case, that of THF, experimental data have been obtained for the binding of a third ligand.

Experimental Section

The laser ablation high-pressure mass spectrometer (LAHPMS) currently used is a somewhat modified version of that described previously by Bouchard *et al.*[12b] The basic design is that of the conventional high-pressure mass spectometer (HPMS) of Kebarle,[16] which utilizes a high-pressure (5 to 10 Torr) source with two 100−200 μm apertures for the electron entrance and ion exit arranged in a 90° geometry. Ions generated by 2000 V electrons are allowed to diffuse from the ion source into the ion acceleration optics of the mass spectrometer. In the process, these ions undergo 10^5-10^6 collisions, thermalizing them as well as allowing reactions with other ligands in the bath gas. Using a pulsed electron gun leads to time-resolved experiments and the observation of residence time distributions (RTD). For equilibrium studies time resolution is necessary since the ions often need on the order of 1 ms to reach steady-state relative abundances.

Laser ablation, using either a Nd:YAG or excimer laser, has been shown to be able to generate metal neutrals and ions from virtually all available metal targets.[17] In addition, the pulsed

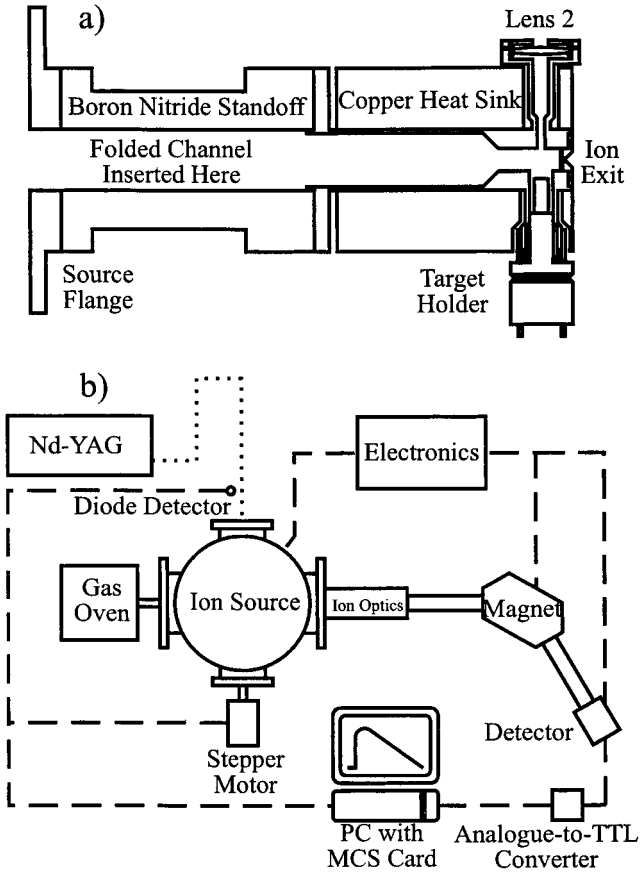

Figure 1. (a) Schematic of the ion source. (b) Schematic of the laser ablation high-pressure mass spectrometric apparatus.

nature of the laser fits very nicely with the necessary time resolution of the experiments. The merging of the two techniques is accomplished by introducing a metal rod into the ion source 90° to both the electron entrance and the ion exit apertures and positioning a focusing lens directly opposite the metal target (Figure 1a). This particular arrangement produces metal ions directly inside the ion source where they are subsequently thermalized. Depending on the bath gas and reactant gas mixture, various equilibria can be studied as will be detailed below.

The mass spectrometer portion of the apparatus (Figure 1b) is a modified V. G. Micromass, Ltd. 16 HC single-focusing instrument. Of the original instrument, only the vacuum housing, the magnet, and the electronics controlling the magnet and some of the vacuum pumps have been retained. The retained source housing now contains ion optics and the first field free region. The new ion source housing was constructed by the University of Waterloo Science shop utilizing an Alaria chamber and flange design. The inside dimension of the source housing is 33 cm providing abundant space for the ion source and heating mantle. The source housing is pumped by a 2300 L/s Edwards Diffstak series 250 diffusion pump, and the first field free region is pumped by a 800 L/s Edward EO6 diffusion pump. Both can be isolated by a butterfly valve. The magnet and detector regions are pumped by a 150 L/s Edwards EO2 diffusion pump. These regions can be isolated from the main housing by a gate valve. The advantage of this pumping arrangement is that the source housing can be vented by simply isolating it from the pumps and the detector region, facilitating the metal target changing greatly.

The ion source is essentially identical to the ion sources used at Waterloo in other HPMS instruments[18] except for three major modifications (Figure 1a). The first modification is the attach-

ment of a rotatable metal target holder and a lens on the ion source. Of note here is the vacuum seal of the target holder. A two stage teflon seal has been used in place of a Viton O-ring since the Teflon seal does not need any lubricant at high temperature. The second modification is the boron nitride standoff which contains a folded gas channel. This modification has become necessary since Argon is used currently as the bath gas, and its breakdown pressure is in the same range as that used in the source. With this modification the effective standoff between ground and the source high voltage is approximately 60 cm. Nitrogen, which was used earlier, has been implicated in the formation of ammonia, a strong clustering agent, during the laser pulse with the hydrogen embedded in many of the transition metals. The third modification is the copper mantle surrounding the source and gas entry line that acts as the heat sink. It now contains air channels that are connected with copper tubing to the outside to allow air cooling of the ion source. This offers the advantages of faster temperature changes and an expanded temperature range to colder temperatures. Since the original electron entrance aperture has been left in place, an electron gun was also added to the instrument and can be used for ion focusing as well as calibration purposes. In this arrangement, the instrument is typically run with an acceleration voltage of 2000V yielding a maximum *m/z* of about 1250 with an approximate resolution of 350.

The laser used in these experiments is a Quanta Ray DCR-1A pulsed Nd:YAG laser. Both the fundamental 1064 nm and the frequency-doubled 532 nm light were used for laser ablation. The light is guided with a set of uncoated UV grade fused silica prisms through a 6 mm window into the source housing, and a double-lens telescope arrangement is used for focusing. One of the focusing lenses is used in the sealing of the ion source, the other lens is outside the source housing and can be manually adjusted. The spot size of the laser on the target ranges from 0.2 to 0.5 mm and was adjusted for optimum ion signal intensity. Some metals, such as, for example, aluminum, generated more ions with less target damage when larger spot sizes were used. In addition, neutral density filters were added into the beam path to attenuate the light intensity to an optimal range for our conditions. In order to provide the laser with a new spot the target is rotated *via* a stepping motor by $1^2/_3°$ providing 216 spots/full rotation. Rotation of the target increases the length of time during which the signal remains stable. After a number of rotations, dependent upon the metal and the laser intensity, the signal deteriorates and the laser is redirected to a new track. Another observation regarding signal intensity is a presumed charge buildup around the ion exit aperture under many ion source conditions. This phenomenon, fairly common under certain conditions in HPMS,[19] leads to low signal intensities since the small charge build up around the aperture is sufficient to hinder ion exit in an otherwise field free ion source.

In laser ablation mode, the laser initiates the timing events and a light sensitive diode was used as the trigger for both the detection electronics as well as the stepping motor. The detection electronics are very similar to those used in other HPMS instruments and details have been published elsewhere.[18a]

Data collection involves monitoring the residence time distribution (RTD) of the reactant ion and the association product ion. If the two ions achieve equilibrium, the later segment of the RTDs become parallel. The ratio of the normalized RTDs in the region where equilibrium is reached is used as a measure of the ratio of the relative concentration of the two ions in the source. From the ratio and the neutral reactant gas concentration the equilibrium constant for the association reaction can be evaluated according to the following equation:

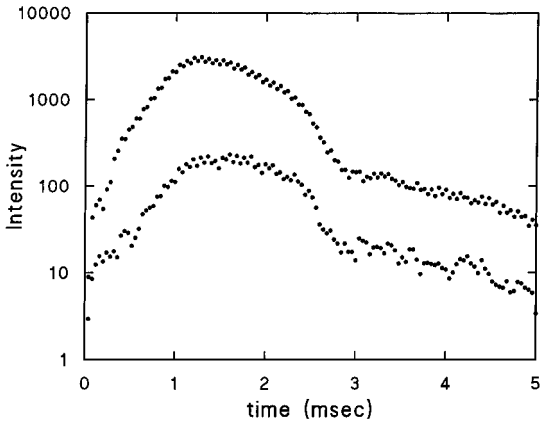

Figure 2. Experimental time-intensity profiles for a second-ligand complexation reaction. Upper points are $Al(CH_3OCH_3)^+$. Lower points are $Al(CH_3OCH_3)_2^+$.

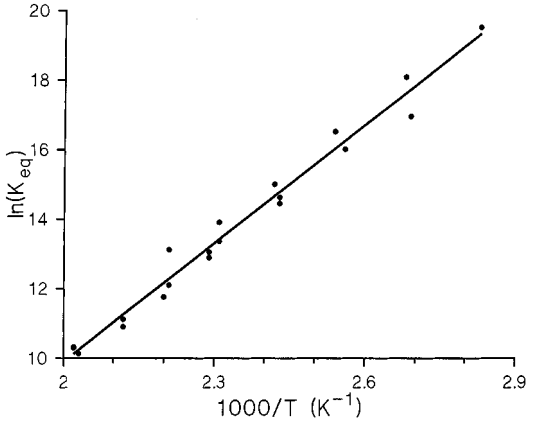

Figure 3. Van't Hoff plot for the second complexation of Al^+ and $(CH_3)_2O$.

$$K_{eq} = \frac{I(\mathrm{AB})p_0}{I(\mathrm{A})\,p(\mathrm{B})}$$

where $I()$ is the ion intensity of the cluster AB and the monomer A, p(B) is the pressure of neutral B, and p_0 is standard pressure.

By heating or cooling the source, the equilibrium constant can be studied as a function of temperature. The result can be displayed in a van't Hoff plot where the slope and the intercept yield the reaction enthalpy and the reaction entropy, respectively. Because of the less stable signals resulting from laser ablation, compared to the more common pulsed electrun gun HPMS experiments, the experimental uncertainties in $\Delta H°$ and $\Delta S°$ are somewhat greater at $\pm$ 1.0 kcal mol^{-1} and $\pm$ 5 cal mol^{-1} K^{-1}, respectively.

Figure 2 shows a typical example of an RTD for the association reaction of $Al[(CH_3)_2O]^+$ plus $(CH_3)_2O$. For this reaction the data had to be collected at near threshold conditions since conditions that would yield large ion intensities did not achieve the necessary equilibrium. Figure 3 shows the corresponding van't Hoff plot for this association reaction with a temperature range from 80 to 223 °C.

Computational Section

Calculations[22a] were performed on $Al[OCH_2]^+$ and various isomers of $Al[CH_3CN]_n^+$ and $Al[(CH_3)_2O]_n^+$ (n = 1 and 2). Except where specifically indicated, all calculations were done at the frozen core MP2 level. A variety of basis sets were used. In most cases, the standard 6-31G* basis was used for geometry optimizations and vibrational frequency calculations. For the

TABLE 1: Calibration Calculations on Al(H_2CO)$^+$

method	Al−O[a]	O-C[a]	AlOC[b]	total energy[c]	D_e[d]	D_0[d]	ΔH°_{298}[d]	ΔS[e]
HF								
3-21G C_{2v}	1.929	1.234	180.0	−353.63480	40.6	39.4	−40.0	−23.9
6-31G* C_{2v}	2.032	1.211	180.0	−355.56526	29.4	28.5	−28.8	−19.7
6-311+G(2d,2p) C_{2v}	2.025	1.205	180.0	−355.61777	26.5	25.7	−26.5	−25.0
6-311+G(2d,2p) C_s	2.025	1.205	170.0	−355.61779	26.5	25.6	−25.9	−18.3
aug-cc-pVTZ C_{2v}	1.998	1.205	180.0	−355.63326	27.9	27.0	−27.3	−19.9
MP2(FC)								
3-21G C_{2v}	2.034	1.262	180.0	−353.86471	34.5	33.3	−33.7	−21.8
6-31G* C_{2v}	2.071	1.238	180.0	−355.89316	29.9	28.9	−29.7	−25.8
6-311+G(2d,2p) C_{2v}	2.097	1.230	180.0	−356.00403	25.9	25.0	−25.7	−24.7
6-311+G(2d,2p) C_s	2.101	1.231	155.9	−356.00415	25.9	24.8	−25.1	−19.4
aug-cc-pVTZ C_{2v}	2.065	1.230	180.0	−356.06186	27.7	26.8[g]	−27.1[g]	−19.9[g]
MP2(FC)//HF[f,g]								
aug-cc-pVTZ C_{2v}				−356.06044	28.1	27.2	−27.5	−19.9

[a] Distances in angströms. [b] Angles in degrees. [c] In Hartrees. [d] In kcal mol^{-1}. [e] In cal mol^{-1} K^{-1}. [f] Single-point MP2 calculation at the HF-optimized geometry with the same basis set. [g] Using the HF frequencies.

TABLE 2: Calculated Components of Thermal Energy and Entropy for 5a, d, and 3a Dimethyl Ether, and Al$^+$ at the MP2/6-31G* Level

	5a	5d	3a	CH_3OCH_3	Al^+
ZPVE[a] (E_{therm}^0)	105.50	104.67	52.48	51.58	
E_{therm}^{298}					
total	112.83	112.47	56.34	54.25	
electronic	0.00	0.00	0.00	0.00	
translational	0.89	0.89	0.89	0.89	0.89
rotational	0.89	0.89	0.89	0.89	0.89
vibrational	111.05	110.69	54.56	52.47	
S^{298}[b]					
total	106.19	116.42	76.93	64.26	35.80
electronic	0.00	0.00	0.00	0.00	0.00
translational	40.24	40.24	38.78	37.41	35.80
rotational	28.66	29.99	25.44	22.06	
vibrational	37.29	46.19	12.71	4.80	

[a] ZPVE = zero-point vibrational energy (in kcal mol^{-1}). [b] In cal mol^{-1} K^{-1}.

study of the [Al, C_2, H_6, O]$^+$ potential energy surface (PES), insertion of Al^+ into a C−H bond was studied, requiring the use of polarization functions on hydrogen atoms for better accuracy. Therefore, the 6-31G** basis was used. Since noncovalently bound isomers of Al[$(CH_3)_2O]_2^+$ include hydrogen bonding between the two dimethylether molecules, calculations were also performed with the 6-31G** basis in this case. Finally, in order to add more flexibility to the description of the bonding interaction and also to reduce basis set superposition error (BSSE),[22b] single-point calculations were run with either the 6-311G(2d,2p) or 6-311+G(2d,2p) bases.

Calibration calculations were performed on the Al[OCH_2]$^+$ complex, since this case is used to anchor the absolute scale of Al^+ affinities (see below). Results are reported in Table 1. Whenever comparable, they are in good agreement with literature results.[12,15] It can be seen that the Al−O bond distance is systematically underestimated at the HF level, especially when using the 3-21G basis set which leads to a large BSSE, yielding a grossly overestimated bond dissociation energy (BDE). In order to obtain an accurate BDE, rather large basis sets must be used. On the other hand, Hartree−Fock (HF) values are in good agreement with the MP2, due to an essentially electrostatic binding mode complemented with a cancelation of errors on Al[OCH_2]$^+$ and OCH_2. This leads to accurate values also at the MP2//HF level. Alcamí *et al.*[15b] showed that the MP2, MP3, and MP4 levels of perturbation theory yield very similar BDEs, with the MP4 value larger than the MP2 by 0.3 kcal mol^{-1}. Furthermore, we have checked that the frozen core approximation on Al^+ leads to a very small underestimation of the computed BDE of 0.1 kcal mol^{-1}. Therefore, on the basis of the MP2/aug-cc-pVTZ value of −27.1 kcal mol^{-1}, we can provide an accurate estimate for the value of ΔH° for reaction 4 at 298 K of −27.5 kcal mol^{-1}. This is in good agreement with the experimental value of -27.5 ± 2.5 kcal mol^{-1} reported below. A side problem encountered in these calculations is due to the fact that with some of the basis sets used, the C_{2v} structure in which the AlOC skeleton is linear turned out to be a transition state for the interconversion between two symmetry equivalent bent structures of C_s symmetry. As already discussed by Stöckigt,[13e] this is a computational rather than physical issue. However, the very small vibrational frequencies obtained in such cases (see the HF and MP2 results with the 6-311+G(2d,2p) basis in Table 1) lead to rather large uncertainties in the computed entropies. A reliable value for the entropy variation of reaction 4 appears to be −20 cal mol^{-1} K^{-1}.

As discussed below, it was deemed important to explore regions of the PES for Al[$(CH_3)_2O]_2^+$ in which the second dimethylether molecule interacts with the first one rather than with the metal cation. Traditional quantum chemistry methodology is inadequate for such a purpose, for several reasons. First, interactions between neutral molecules, in which dispersion forces play a large role, require highly sophisticated wave functions which would be intractable for a system this large. Second, the use of local minimization techniques could easily lead to bias in favor of some of the extrema on the PES and miss others. We have used instead a combination of semiempirical calculations specifically devised for intermolecular interactions, and simulated annealing techniques to thoroughly explore the PES. These techniques have been extensively discussed and applied elsewhere,[20] and the reader is referred to these sources for details. We have successfully extended this approach to systems involving positive ions.[21] Parameters had to be determined for the aluminium atom. The van der Waals parameter, and the atomic parameter involved in the repulsion, dispersion, and dispersion−exchange components of the interaction energy, were determined from *ab initio* calculations on AlAr at the MP2 level using a large basis set. In such a species, the other energy components (electrostatic and polarization) are negligible. The Al−O bond polarizability was determined by fitting the ab initio molecular polarizability of Al[$(CH_3)_2O]_2^+$, computed using an appropriately extended basis set, with bond increments. Final values are R(Al) = 1.549 Å, k(Al) = 5.018 and a(Al−O) = 25.474 au.

In the present case, two types of minima were located on the Al[$(CH_3)_2O]_2^+$ PES, and transition structures connecting these minima were also determined. We have further confirmed the relevance of such calculations for the system under study by reoptimizing the two minima at the MP2/6-31G* level. The

good agreement between results obtained by both methods is very encouraging for future studies. It must be emphasized that, in such a case, the determination of ab initio minima without the semiempirical structures as starting points would be an extremely tedious task, and would by no means guarantee that all relevant structures have been located.

Most calculations were run on RS6000 workstations, while the largest frequency calculations had to be run on a Cray C98. All calculations were done with the Gaussian94 package.[22a]

Results and Discussion

1. Single Ligand Complexation Energetics. In early ICR experiments Staley *et al.*[10] demonstrated that reaction of Al^+ with ethanol leads readily to the formation of a $Al[H_2O]^+$ complex, eq 1. Subsequent reaction with other ligand species

$$Al^+ + C_2H_5OH \rightarrow Al[OH_2]^+ + C_2H_4 \quad (1)$$

$$Al[OH_2]^+ + L_1 \rightarrow Al[L_1]^+ + H_2O \quad (2)$$

$$Al[L_1]^+ + L_2 \rightleftharpoons Al[L_2]^+ + L_1 \quad (3)$$

present in the ICR cell lead to the observation of Al^+ transfer equilibria, eqs 2 and 3 from which a scale of $\Delta\Delta G°$ values for Al^+ binding could be obtained. With the assumption of little or no entropy change accompanying Al^+ transfer, this gave a $\Delta\Delta H°$ ordering corresponding to a scale of relative Al^+ binding energies to species binding to Al^+ as weakly as CH_3CHO. Gal *et al.*[11] have successfully generated Al^+ complexes of a variety of bases by direct clustering at low pressures and have extended this Al^+ binding scale to more weakly bonding ligands such as CH_3OH and CH_2O as well as providing data for many additional compounds.

Using the new equilibrium experimental method described above attempts were made to examine the association of a single molecule with Al^+. For organic bases, such as those in the Staley scale, the association equilibria between Al^+ and a single-ligand molecule were not possible since the first and second ligand molecules were so strongly bound to Al^+ that, even at the highest temperatures attainable in the apparatus, the bare Al^+ disappeared rapidly after the laser pulse and only the singly and doubly ligated species were present. The sole exception to this situation was for CH_2O, where at 250 °C equilibrium between Al^+ and $Al[OCH_2]^+$ was observable, eq 4.

$$Al^+ + CH_2O \rightleftharpoons Al[OCH_2]^+ \quad (4)$$

The value of $\Delta G°_{523}$ of -17.1 kcal mol^{-1} obtained can be coupled with the calculated value of $\Delta S°$ of -20 cal mol^{-1} K^{-1} to yield a bond energy for Al^+ to CH_2O of 27.5 ± 2.5 kcal mol^{-1}. The much larger than normal error bar, relative to most HPMS measurements, arises from the fact that only a single temperature was examined thus necessitating an estimate of $\Delta S°$ which will have a potential uncertainty of ± 5 cal mol^{-1} K^{-1}. Nonetheless, this value for CH_2O permits the relative free energies obtained by Staley[10] and Gal[11] to be converted to approximate absolute values. In general the values reported by Staley[10] can be converted to absolute binding energies by the addition of 37 kcal mol^{-1}. A selection of these values, so derived, is summarized in Table 3. Also included for comparison are the values obtained by *ab initio* calculation for a few of the single-ligand complexes. The values of Sodupe and Bauschlicher for CH_2O and $(CH_3)_2CO$ of 27.4 and 41.2 kcal mol^{-1}, respectively,[23] can be seen to be in excellent agreement with the experimental results.

TABLE 3: Experimental and Computed ΔH and ΔS Values for $Al^+ + L \rightarrow Al[L]^+$ Reactions

	experimental enthalpies[a]	theoretical enthalpies (others)	theoretical enthalpies (this work)[b]
CH_3F	-21.5 ± 2.0[c]	-22.3[d]	
H_2CO	-27.5 ± 2.5[c]	-26.9[d] (-27.2)[e]	-27.5 (-19.9)
MeOH	-33.4	-30.2[d]	
EtOH	-36.6	-32.3[d]	
MeCN	-36.2	-33.4[d]	-35.0 (-22.0) [**2**]
Me_2O	-37.9	-32.0[d]	-36.6 (-23.1) [**3a**]
Me_2CO	-42.3	-41.7[e]	
Et_2CO	-45.7		

[a] The experimental enthalpies are derived from the Staley scale (ref 10) anchored to the formaldehyde value from this work unless otherwise noted. All enthalpy values in this table are in kcal mol^{-1}. [b] Entropy values in cal mol^{-1} K^{-1} are given in parentheses. [c] This work. [d] Reference 15a. [e] Reference 12b.

1 **2**

Figure 4. Optimized structures of $Al(H_2CO)^+$ **1** and $Al(CH_3CN)^+$ **2** at the MP2/6-311+*G*(2d,2p) level.

The nature of the bonding between Al^+ and simple ligands is a matter of some current interest. For example, Schwarz *et al.*,[13b] as well as Watanabe and Iwata,[14] have shown that for a single H_2O molecule bound to Al^+ the simple electrostatic adduct is more strongly bound than an inserted $HAlOH^+$ species by ~10 kcal mol^{-1}. However these two structures are connected by a transition state which lies ~35 kcal mol^{-1} higher in energy than that of the separated Al^+ and H_2O. Conversely, the latter authors have shown that when a second H_2O molecule adds to $Al[OH_2]^+$ the simple association to the Al^+ center is less stable than an inserted $[HAlOH]OH_2^+$ complex by ~20 kcal mol^{-1}. This possibility of the existence of both electrostatic and inserted complexes is of some considerable relevance to the current work in view of the observation by Staley *et al.*[10] of elimination of C_2H_4 in the reactions of Al^+ with C_2H_5OH and $(C_2H_5)_2O$. This elimination presumably involves insertion of the metal ion into a C−O bond without an activation energy in excess of the total energy of reactants. As a result it was deemed important to examine the possibility of both types of bonding in representative ligand species using high level *ab initio* calculations. Acetonitrile, CH_3CN, was chosen as a prototypical species in which only electrostatic complexation was likely to occur and dimethyl ether as a candidate for which both possibilities appear to be plausible. Calculations were also carried out for $Al[CH_2O]^+$ in order to aid in the derivation of the absolute Al^+ affinity scale as described above, resulting in $\Delta H°_{298}$ and $\Delta S°$ values of 27.5 kcal mol^{-1} and -20 cal mol^{-1} K^{-1}, respectively.

The MP2/6-31G*-optimized geometry for the $Al[CH_3CN]^+$ complex **2** is shown in Figure 4. The Al^+−N distance of 2.157 Å is 0.12 Å shorter than the bond distance found in the analogous HCN complex[13c] consistent with its greater bond strength. The binding energy (D_0) computed at the MP2/6-311+*G*(2d,2p)//MP2/6-31G** level is 34.8 kcal mol^{-1}, which can be compared to the value of 33.4 kcal mol^{-1} obtained by Smith *et al.*[15a] In order to compare the computed and experimentally measured values, thermal and ΔPV corrections must be made. This leads to a computed $\Delta H°_{298}$ of 35.0 kcal mol^{-1}, which is in good agreement with the derived experimental value of 36.2 kcal mol^{-1}. The entropy change for the addition of CH_3CN to Al^+ is computed to be -22.0 cal mol^{-1}

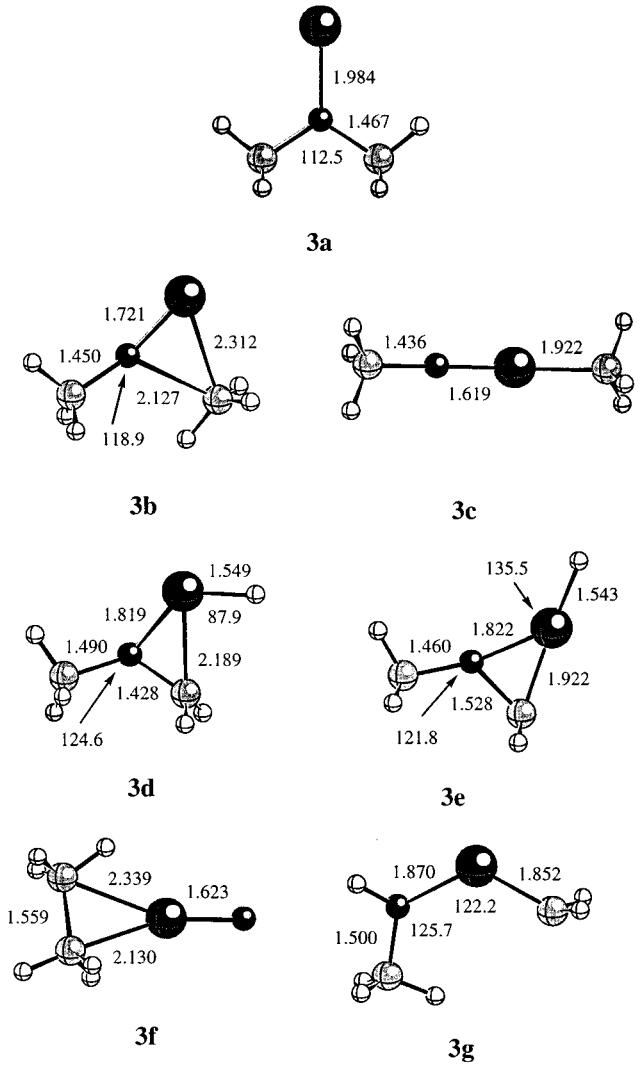

Figure 5. Main geometrical parameters of the optimized extrema (**3a**−**g**) on the $[Al, C_2, H_6, O]^+$ potential energy surface at the MP2/6-31G** level.

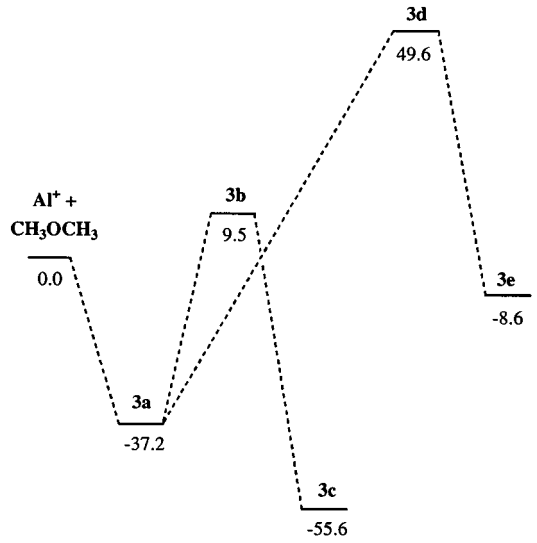

Figure 6. Potential energy profile for the interaction of Al^+ with dimethyl ether, computed at the MP2/6-311+*G*(2d,2p)//MP2/6-31G** level.

K^{-1}, which is typical for the reaction of an atomic ion with a polyatomic molecule.[24]

Similar computations were carried out for the complex between Al^+ and $(CH_3)_2O$ together with other possible extrema on the $[Al,C_2,H_6,O]^+$ potential energy surface (see Figures 5 and 6). The simple association complex **3a** is bound by 37.2 kcal mol^{-1}. The Al^+ bond distance is again shorter than that found in the analogous H_2O complex by 0.15 Å,[13b] consistent with the approximately 9 kcal mol^{-1} stronger bond. The corresponding 298 K bond enthalpy of 36.6 kcal mol^{-1} is again in good agreement with the derived experimental value of 37.9 kcal mol^{-1}. However the electrostatic complex is not the global minimum on the PES. Insertion of Al^+ into one of the C−O bonds leads to structure **3c**, which is bound by 55.6 kcal mol^{-1} relative to separated Al^+ and $(CH_3)_2O$. The Al−O bond in **3c** is significantly shorter than that in the electrostatic complex **3a** consistent with the fact that a true covalent bond has been formed. The analogous Al−C bond length must also have a strong covalent character corresponding to sp hybridization on Al^+ which is in agreement with the linear C−Al−O structure. **3a** and **3c** are separated by a transition structure, **3b**, which lies 9.5 kcal mol^{-1} above the separated reactants. The insertion of Al^+ into a C−H bond has also been considered, leading to structure **3e** which is bound by 8.6 kcal mol^{-1} relative to separated fragments. Although bound, this structure is considerably less stable than either **3a** or **3c**. Therefore, it is not surprising that the transition state **3d** connecting **3a**,**e** is of high energy, 49.6 kcal mol^{-1} above separated fragments. Structures **3f**,**g** are not bound with respect to Al^+ and $(CH_3)_2O$ (+ 9.4 and 15.4 kcal mol^{-1}, respectively) and therefore are not expected to play any role in the reactions considered here.

It is instructive to compare the PES of Figure 6 to that for $Al^+ + H_2O$. As noted above the inserted complex $HAlOH^+$ is *less* stable than the electrostatic complex in the latter case. Concomitantly, the barrier height, 35 kcal mol^{-1}, for the insertion process is significantly higher than that derived here for $(CH_3)_2O$, 9.5 kcal mol^{-1}. This leads to the conclusion that the observation of the spontaneous elimination reaction of Al^+ with C_2H_5OH and $(C_2H_5)_2O$ is probably the result of the fact that the barrier for insertion into the C−O bond in each of these cases lies below the energies of the respective separated reactants.

2. Second Ligand Complexation Energetics. As noted above for most of the organic ligands examined in the present work the binding energies of the first ligand to Al^+ were sufficiently strong that no direct clustering equilibrium could be observed. However, under the typical HPMS experimental conditions, the one and two ligand species were readily observable and the associated equilibrium measurements were carried out. The thermochemical data derived from these experiments are summarized in Table 4. From a comparison of the data of Tables 3 and 4 it can be seen that there is a general reduction of 10−15 kcal mol^{-1} for the binding energy of the second ligand relative to the first. This tendency has been previously noted in a combined experimental and *ab initio* study of the binding of Al^+ to CH_2O and $(CH_3)_2CO$.[12b] The entropies are also of some interest. The addition of CH_3CN to the single ligand complex, eq 5 is accompanied by a −20 cal mol^{-1} K^{-1}

$$Al[CH_3CN]^+ + CH_3CN \rightleftharpoons Al[CH_3CN]_2^+ \qquad (5)$$

entropy change which is notably less in magnitude than the corresponding change observed for the ketones or ethers investigated. Previous calculations[12,14] have shown that a second ligand binds to the Al^+ center with an acute L-Al−L bond angle, which in the case of bulky ligands, leads to a rather unfavorable entropy change due to steric hindrance of internal rotations. The CH_3CN result could then be understood on the basis of a linear Al−N−C−C arrangement which minimizes ligand−ligand

TABLE 4: Measured and Computed ΔH and ΔS Values for $Al[L]^+ + L \rightarrow Al[L]_2^+$ Reactions

	experimental		theoretical	
ligand	ΔH^a	ΔS^b	ΔH^a	ΔS^b
acetone	−28.3	−30.7	−26.8[c]	−28.6[c]
acetone-d_6	−28.2	−31.0		
cyclopentanone	−28.7	−32.0		
diethylether	−30.8	−45.9		
tetrahydrofuran	−31.0	−36.3		
tetrahydropyran	−30.6	−35.5		
acetonitrile	−22.2	−20.1	−24.7	−18.6 [**4a**]
dimethyl ether	−22.6	−25.4	−26.7	−35.0 [**5a**]
formaldehyde	$\Delta G° = -13.6$ kcal mol^{-1} at 250 °C			
1,4-dioxane	$\Delta G° = -11.9$ kcal mol^{-1} at 170 °C			

[a] All enthalpies are in kcal mol^{-1}. [b] All entropies are in cal mol^{-1} K^{-1}. [c] Values are taken from reference 12b. The best estimate is given as 23 kcal mol^{-1} based on a basis set trend comparison with the analogous Al[formaldehyde]$^+$ + formaldehyde reaction. The entropy value was determined at 300 K.

interaction. This is borne out by the *ab initio* calculations described below. A comparison of the entropy data for diethyl ether and THF or THP shows that the cyclic ethers have a less negative entropy change accompanying the addition of the second ligand. In the cyclic cases no free rotation about the C−C and C−O bonds is possible in the free molecule. Thus, upon complexation no internal rotations are restricted regardless of the proximity of the two ligands. In contrast each $(C_2H_5)_2O$ molecule has two C−C and two C−O internal rotations some of which can become significantly restricted when the second ether molecule adds to $Al[(C_2H_5)_2O]^+$. In addition in the two-ligand complex, the Al−O bond rotations will also become restricted.

An initial inspection of the experimental ΔH and ΔS data for dimethyl ether suggested that these values were both rather low in magnitude, leading to the speculation that a structure other than the electrostatic two-ligand complex might be involved at the temperatures where the equilibrium was examined. For this reason an extensive computational search of the PES for $Al[(CH_3)_2O]_2^+$ was deemed desirable. Included in this search were structures in which the second ligand interacts with the first ligand instead of with the metal ion. Such structures will be termed nonclassical as opposed to classical structures in which both ligands interact directly with the metal ion *via* the most basic heteroatom site.

The MP2/6-31G*-optimized geometry for the classical $Al[CH_3CN]_2^+$ complex, **4a**, is shown in Figure 7. As seen previously for other diligated Al^+ complexes, the second ligand molecule is found to bind to the metal center with an acute N−Al−N bond angle of, in this case, 82°. This is due to the fact that binding of the first molecule induces a polarization of the metal $3s^2$ electrons away from the ligand. If the second molecule binds with an acute angle it can benefit from this polarization by having a reduced metal−ligand electron repulsion. The Al−N distance of 2.191 Å is slightly longer than that in the single-ligand complex **2** of 2.169 Å. The internal structure of CH_3CN does not change from the one to the two-ligand complex. In order to minimize ligand−ligand repulsion the Al−N−C bond angle deviates from linearity at 164°. The magnitude of this reduction in bond angle remains small because this leads to imperfect alignment of the charge on Al^+ and the dipole moment of CH_3CN. The resulting structure, in which the two CH_3 groups are sufficiently separated that there is very little interaction between them, serves to explain the small magnitude of the entropy change experimentally observed. The value of $\Delta H°_{298}$ of −24.7 kcal mol^{-1}, obtained for clustering

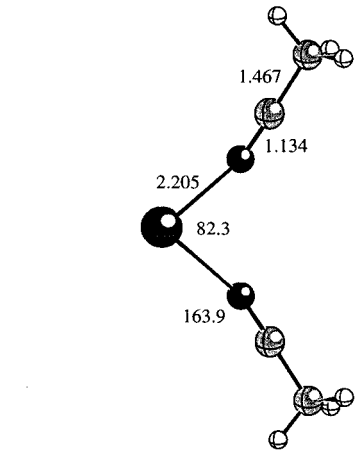

4a

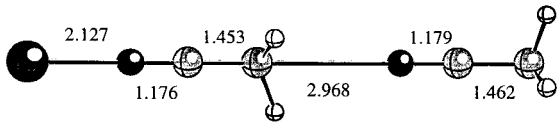

4b

Figure 7. Main geometrical parameters of the optimized structures for $Al(CH_3CN)_2^+$ (**4a**−**b**) at the MP2/6-31G* level.

reaction 5, (D_e computed at the MP2/6-311+*G*(2d,2p)//MP2/6-31G* level and thermal corrections computed at the MP2/6-31G* level) compares very favorably with the experimental observation of −22.2 kcal mol^{-1}. Similarly the calculated entropy change of −18.6 cal mol^{-1} K^{-1} is in excellent agreement with the experimental value of −20 cal mol^{-1} K^{-1}. In addition, calculations were carried out for a nonclassical structure in which the nitrogen atom of the second molecule interacts with the methyl group of the initially bound acetonitrile. The optimized structure is shown as **4b** in Figure 7. This isomer lies 16.3 kcal mol^{-1} higher in energy than **4a** at the MP2/6-311*G*(2d,2p)//MP2/6-31G* level and, therefore, should not be the species observed at equilibrium in the present experiments.

As noted above, since the experimental values of $\Delta H°$ and $\Delta S°$ obtained for the addition of the second $(CH_3)_2O$ appeared to be anomalously low, it was felt to be important to explore thoroughly the possibility of different types of bonding in this complex. The normal *ab initio* procedures for exploring a PES are inadequate in this case since it would be too computationally demanding and also because the nonclassical types of bonding possible are too numerous to search for using the conventional local methods. As a result, a search based on a simulated annealing algorithm was carried out in conjunction with energy calculations using semiempirical techniques.[20,21] The most energetically favorable regions of the potential energy surface were then investigated further using conventional quasi-Newton optimization techniques. Similar methods were then used to search for transition states connecting the local minima thus found. The final transition state structures were obtained by the chain method.[20e] Since this overall procedure uses frozen electron densities for the fragments, it is known not to be adequate for classical complexes in which there is some degree of covalent bonding and therefore it was used only for the nonclassical possibilities. The more stable of the two types of minima on the semiempirical surface corresponds to a structure in which the oxygen atom of the second dimethyl ether molecule interacts with one of the C−H bonds on each of the methyl groups of the initially bound ether ligand. This species lies 9.1 kcal mol^{-1} below the energy of separated fragments. There are several, nearly equivalent, structures of this type depending

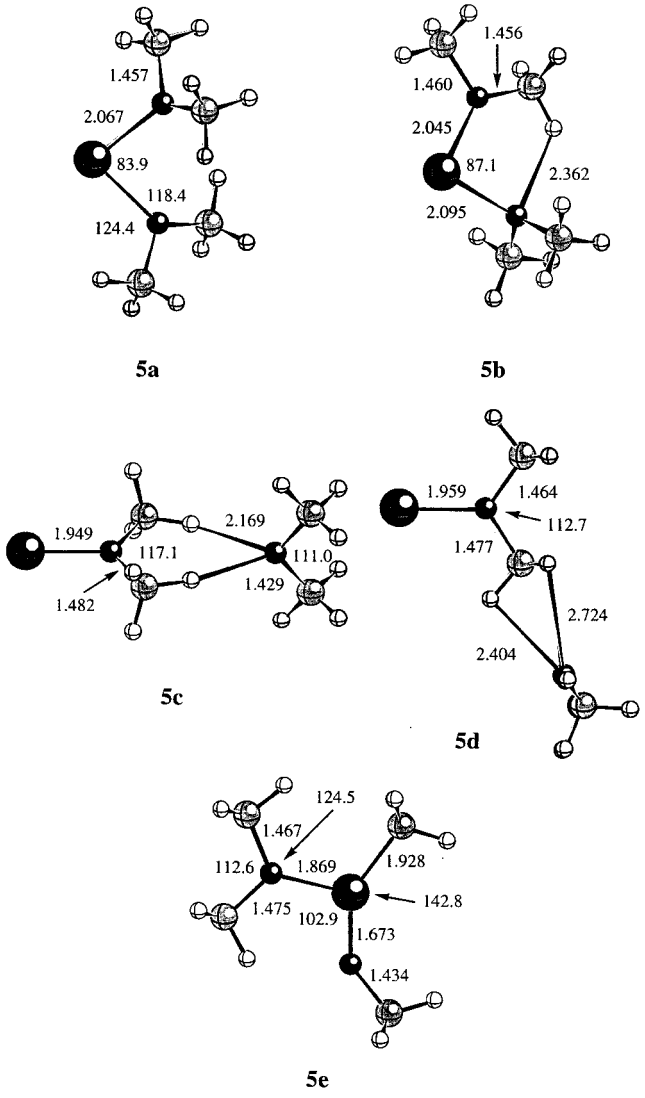

Figure 8. Main geometrical parameters of the optimized structures for $Al(CH_3OCH_3)_2^+$ (**5a**−**d**) and $CH_3OAl^+CH_3(CH_3OCH_3)$ (**5e**) at the MP2/6-31G** level.

upon which pair of methyl group hydrogens interacts with the oxygen atom of the approaching molecule. The transition states connecting these structures correspond formally to internal rotation of the methyl groups of the initially bound dimethyl ether molecule. One such structure was refined and found to lie 0.8 kcal mol^{-1} higher in energy than the corresponding minima. The second type of minimum corresponds to the interaction between the oxygen atom of the incoming second ligand and all three C−H bonds of one methyl group of the initially bound ligand. This species, formally resembling a backside attack type of complex, lies 7.5 kcal mol^{-1} below separated fragments. Since there are two equivalent methyl groups in the initially bound dimethyl ether there are two such minima which are connected by a transition state lying 0.3 kcal mol^{-1} higher in energy. Thus the nonclassical part of the potential energy surface appears to be relatively flat.

The two nonclassical minima described above were further refined using standard *ab initio* techniques. The two nonclassical structures **5c** and **5d** thus obtained, together with two classical structures found directly by *ab initio* methods are shown in Figure 8.

In both *non*classical isomers **5c** and **5d**, the dimethylether which is directly bound to Al^+ is very similar to that found in **3a**. Weak H-bond interactions are established with the oxygen atom of the second molecule. In **5c** the C−H···O structure is closer to being linear than in **5d**, leading to significantly shorter O···H distances. However, there are three interactions in **5d** *versus* two in **5c**, resulting in very similar energies for both structures. It is likely that some of the binding in such species arises from long-range attraction between the second dimethylether molecule and the charge on Al^+.

TABLE 5: Computed D_e for 5a−e

level	5a[a]	5b	5c	5d	5e
MP2/6-31G*	39.8	40.9	59.8	59.6	0.0
MP2/6-31G**	39.9	41.0	59.7	59.3	0.0
MP2/6-311*G*(2d,2p)//MP2/6-31G**	47.2	48.4	66.3	65.4	0.0
MP2/6-311+*G*(2d,2p)//MP2/6-31G**	47.6				0.0

[a] All energy values are relative to **5e** and given in kcal mol^{-1}.

Overall there is very good agreement between the well depths of the nonclassical structures whether computed using semiempirical or *ab initio* methods. The values for the binding energies (D_e) of each of the classical and nonclassical structures (**5a**−**d**) are summarized in Table 5. The corresponding values of $\Delta H°$ and $\Delta S°$ have been computed for the more stable of each of the pairs of classical and nonclassical isomers, **5a** and **5d**. The value of $\Delta H°$ to yield **5a** is greater than the experimental value by ∼4 kcal mol^{-1}. This is similar to the difference of 2.5 kcal mol^{-1} found for the *ab initio* and experimental values for the analogous complex of acetonitrile. The nonclassical isomers **5c** and **5d** lie sufficiently above **5a** in energy that such species can be ruled out as being the one which is experimentally observed. On this basis, therefore, **5a** would appear to be the most likely structure. However, the entropy data give a value of $\Delta S°$ to form **5a** of −35 cal mol^{-1} K^{-1}, which is significantly greater in magnitude than the experimental value of −25.4 cal mol^{-1} K^{-1}. For this reason some doubt was raised that **5a** was the sole possibility for the species experimentally observed and the further possibility of an insertion of the second dimethyl ether molecule was considered. The structure obtained, **5e**, is considerably lower in energy than any of the isomers considered above, lying 48 kcal mol^{-1} below **5a** in energy at the MP2/6-311+*G*(2d,2p)//MP2/6-31G* level. It is noteworthy that **5e** is more stable than **5a** by 48 kcal mol^{-1}, while the corresponding difference between **3c** and **3a** is only 18 kcal mol^{-1}. This is very reminiscent of the situation recalled above for complexation of one and two H_2O molecules by Al^+. This binding energy is so large that if this species were formed in the present experiments no equilibrium could be observed with the singly ligated complex. This then means that a significant barrier must still exist for the insertion of Al^+ into a C−O bond when a second dimethyl ether molecule adds to the $Al[(CH_3)_2O]^+$ complex, **3a**. In this respect the general features of the proposed PES for the second addition of dimethyl ether (Figure 9) are qualitatively similar to those for the first ether addition (Figure 6). Thus **5a** appears to be the most probable candidate for the experimentally observed species. The experimental and theoretical entropy changes indicate that the experimentally observed species is less constrained than **5a** is computed to be. This might be rationalized on the basis of the very small energy difference between **5a** and **5b** of 1 kcal mol^{-1}. **5b** differs from **5a** by a formation of an intermolecular O···HC interaction, which induces a slight distortion of the O-Al−O bond distances and angle. If a very small barrier exists between these two structures then at the elevated temperatures at which the experiments are carried out, large amplitude motions of the two ligands on a relatively flat portion of the PES may give rise to entropy effects which are not well described by the calculations which pertain only to a single minimum.

3. Third Ligand Complexation Energetics. There are both experimental and *ab initio* data available for clustering of a third

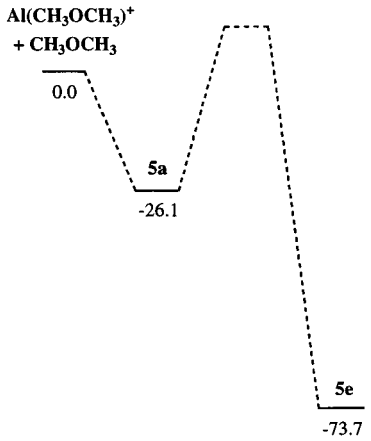

Figure 9. Partial energy profile for $Al(CH_3OCH_3)_2^+$, computed at the MP2/6-311+*G*(2d,2p) //MP2/6-31G** level.

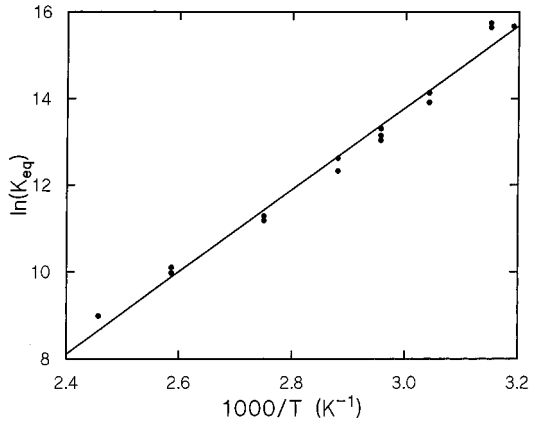

Figure 10. Van't Hoff plot for $Al(THF)_3^+$.

and subsequent water molecules on Al^+. The experimental data of Armentrout *et al.*[25] show a decrease in binding energy for each successive water molecule; however, the difference in binding energy between the second and third molecules is quite small (1 kcal mol^{-1}). The *ab initio* results of Watanabe and Iwata[14] very nicely reveal that this small difference in the second and third binding energies is the result of a structural change in the clusters. With the third addition of H_2O, rather than adding directly to the Al^+ center, this molecule is hydrogen bonded to both of the initially added water molecules. In fact, the calculations show that the third addition of H_2O to the metal center is 3 kcal mol^{-1} less favorable than formation of the hydrogen-bonded complex. This trend in binding energetics suggests that, for the relatively strongly binding organic ligands examined in the present work, equilibrium involving addition of a third ligand should also be observable. In order to investigate the possibility of binding a third ligand directly to the metal center, we selected a case for which no reasonable alternative mode of binding appears to be available. For this reason, H_2O and alcohols have been excluded because of their significant hydrogen-bonding possibilities and carbonyl compounds have been eliminated since there is the possibility of binding the approaching carbonyl oxygen to an already bound carbonyl carbon. Therefore, ethers were considered to be the most suitable types of ligand and, to further maximize the possibility of observation of the third ligand species, an ether with a minimum of steric effects, tetrahydrofuran, was chosen. The van't Hoff plots for the addition of the second and third molecules of THF are shown in Figure 10. The values of $\Delta H°$ and $\Delta S°$ derived for binding the third THF are -18.8 kcal mol^{-1} and -28.8 cal mol^{-1} K^{-1}, respectively. Thus the reduction in binding energy for the third addition is 12 kcal mol^{-1} less than that for the second addition of THF, which in turn, is 13 kcal mol^{-1} less than that for the first addition. In contrast, for additions of H_2O there is almost no difference in the binding energy for the third relative to the second addition of ligand which reflects the change in binding mode of the third H_2O molecule. The $\Delta S°$ for addition of the third THF molecule is actually less than that for the second addition. Using the $Al[H_2O]_n^+$ calculations[14] as a guide, this trend in entropies of addition can be understood from the fact that the Al−L distance will increase with the addition of the third ligand which will thereby reduce the possible ligand−ligand repulsions leading to less hindered rotations about the Al−O bonds.

Conclusion

The experimental data presented above demonstrate that the laser ablation high pressure mass spectrometric method is well suited to the study of metal−ligand complexation energetics. For single-ligand complexes, measurement of the binding energy of Al^+ to formaldehyde permitted the anchoring of existing relative Al^+ affinity scales. For simple organic ligands the first ligand binding energy lies in the range 25−50 kcal mol^{-1}, largely dependent on the gas phase basicity of the ligand concerned. Values derived from *ab initio* calculations are in generally good agreement with the experimental Al^+ affinities. For dimethyl ether a structure in which Al^+ has inserted in a C−O bond is found to be significantly more stable than the simple $Al[(CH_3)_2O]^+$ complexation. However, calculations show that a significant barrier exists which prevents reaction to proceed to the formation of the inserted structure. Previous experiments have shown that reaction of Al^+ with ethanol and diethyl ether do involve insertion without a barrier in excess of the energy of reactants and therefore insertion must be considered to be a common process for larger organic ligands.

The experimental data for two ligand complexes yield bond energies in the range of 20−35 kcal mol^{-1}. The entropy data indicate that significant ligand−ligand interaction can occur. *Ab initio* calculations show that this interaction is due to an acute L-Al−L bond angle (∼80°) for $Al[CH_3CN]_2^+$ and $Al[(CH_3)_2O]_2^+$ as noted previously for H_2O and carbonyl compounds. Again agreement between experimental and calculated $\Delta H°$ and $\Delta S°$ values for the second clustering reaction is generally good. The single significant exception to this is the difference between the two types of data for the $\Delta S°$ for dimethyl ether which can be attributed to the occurrence of a relatively large amplitude motion in this complex. Such effects cannot be adequately taken into account by calculations constrained to considering a single optimum geometry. Nonclassical structures have also been considered for complexes of dimethyl ether and found to be of sufficiently high energy that they do not play a role in the chemistry observed here.

In one case, THF, a three ligand complex has also been examined. The measured $\Delta H°$ and $\Delta S°$ values are consistent with the formation of a pyramidal structure with average Al−O bond lengths greater than those in the two ligand complex.

The present work provides a further example of the beneficial interplay between theory and experiment in the study of gas phase ion chemistry.

Acknowledgment. The financial support of NATO in the form of a International Collaboration Grant greatly faciliated this research. Support of the experimental work at the University of Waterloo was provided by the Natural Sciences and Engineering Research Council of Canada. Support of the computational work at Ecole Polytechnique was provided by the Institut de Developpement et de Ressources en Informatique Scientifique du CNRS (Grant 950543).

References and Notes

(1) For an example involving a metal cation, see: Schwarz, J.; Schwarz, H. *Organometallics* **1994**, *13*, 1518.

(2) (a) Shen, M. H.; Winniczek, J. W.; Farrar, J. M. *J. Phys. Chem.* **1987**, *91*, 6447. (b) Buckner, S. W.; Freiser, B. S. *Polyhedron* **1988**, *7*, 1583. (c) Lessen, D. E.; Asher, R. L.; Brucat, P. J. *J. Chem. Phys.* **1991**, *95*, 1414. (d) Yeh, C. S.; Pilgrim, J. S.; Willey, K. F.; Robbins, D. L.; Duncan, M. A. *Int. Rev. Phys. Chem.* **1994**, *13*, 231.

(3) (a) Armentrout, P. B.; Kickel, B. L. In *Organometallic Ion Chemistry*; Freiser, B. S., Ed.; Kluwer: Dordrecht, 1995; pp 1−45. (b) Sunderlin, L. S.; Wang, D.; Squires, R. R. *J. Am. Chem. Soc.* **1993**, *115*, 12060. (c) Klassen, J. S.; Anderson, S. G.; Blades, A. T.; Kebarle, P. *J. Phys. Chem.* **1996**, *100*, 14218. (d) Hop, C. E. C. A.; McMahon, T. B. *J. Am. Chem. Soc.* **1992**, *114*, 1237.

(4) Dunbar, R. C.; Klippenstein, S. J.; Hrušák, J.; Stöckigt, D.; Schwarz, H. *J. Am. Chem. Soc.* **1996**, *118*, 5277.

(5) (a) Kebarle, P. *J. Am. Soc. Mass Spectrom.* **1992**, *3*, 1. (b) Keesee, R. G.; Castleman, A. W., Jr. *J. Phys. Chem. Ref. Data* **1986**, *15*, 1011. (c) Kemper, P. R.; Hsu, M.-T.; Bowers, M. T. *J. Phys. Chem.* **1991**, *95*, 10600.

(6) Armentrout, P. B. *Acc. Chem. Res.* **1995**, *28*, 430.

(7) (a) Reference 5c. (b) Bushnell, J. E.; Kemper, P. R.; Bowers, M. T. *J. Phys. Chem.* **1993**, *97*, 11628. (c) Kemper, P. R.; Bushnell, J.; von Helden, G.; Bowers, M. T. *J. Phys. Chem.* **1993**, *97*, 52.

(8) (a) Bauschlicher, C. W., Jr.; Langhoff, S. R.; Partridge, H. In *Organometallic Ion Chemistry*; Freiser, B. S., Ed.; Kluwer: Dordrecht, 1995. (b) Bauschlicher, C. W., Jr.; Partridge, H.; Langhoff, S. R. In *Advances in Metal and Semiconductor Clusters*; Duncan, M. A., Ed.; JAI Press, Inc.: Greenwich, 1992.

(9) Parr, R. G.; Yang, W. Density-Functional Theory of Atoms and Molecules; International Series of Monographs on Chemistry 16; Oxford Science Publications: Oxford, 1989.

(10) Uppal, J. S.; Staley, R. H. *J. Am. Chem. Soc.* **1982**, *104*, 1229, 1235.

(11) Gal, J.-F.; Taft, R. W.; McIver, R. T., Jr. *Spectros. Int. J.* **1984**, *3*, 96.

(12) (a) Sodupe, M.; Bauschlicher, C. W., Jr. *Chem. Phys. Lett.* **1991**, *181*, 321. (b) Bauschlicher, C. W., Jr.; Bouchard, F.; Hepburn, J. W.; McMahon, T. B.; Surjasasmita, I.; Roth, L. M.; Gord, J. R.; Freiser, B. S. *Int. J. Mass Spectrom. Ion Processes* **1991**, *109*, 15.

(13) (a) Stöckigt, D.; Hrušák, J. *J. Phys. Chem.* **1994**, *98*, 3675. (b) Hrušák, J.; Stöckigt, D.; Schwarz, H. *Chem. Phys. Lett.* **1994**, *221*, 518. (c) Stöckigt, D.; Holthausen, M.; Koch, W.; Schwarz, H. *J. Phys. Chem.* **1995**, *99*, 5950. (d) Stöckigt, D.; Hrušák, J.; Schwarz, H. *Int. J. Mass Spectrom. Ion Processes* **1995**, *149/150*, 1. (e) Stöckigt, D. *Chem. Phys. Lett.* **1996**, *250*, 387.

(14) Watanabe, H.; Iwata, S. *J. Phys. Chem.* **1996**, *100*, 3377.

(15) (a) Smith, S. F.; Chandrasekhar, J.; Jorgensen, W. L. *J. Phys. Chem.* **1983**, *87*, 1898. (b) Alcamí, M.; Mó, O.; Yáñez, M. *THEOCHEM* **1991**, *234*, 357.

(16) Kebarle, P. In *Techniques for the Study of Ion-Molecule Reactions*; Farrar, J. M., Saunders, W. H., Jr., Eds.; John Wiley & Sons, Inc: NewYork, 1988, pp 221−286.

(17) (a) Conceição, J.; Loh, S. K.; Lian, L.; Armentrout, P. B. *J. Chem. Phys.* **1996**, *104*, 3976. (b) Wu, H-F.; Brodbelt, J. S. *Inorg. Chem.* **1995**, *34*, 615. (c) Ito, O.; Horiki, Y.; Nishio, S.; Matsuzaki. A.; Sato, H. *Chem. Lett.* **1995**, 9. (d) Jordan, R.; Cole, D.; Lunney, J. G.; Mackey, K.; Givord, D. *Appl. Surf. Sci.* **1995**, *86*, 24. (e) Gonzalo, J.; Vega, F.; Afonso, C. N. *J. Appl. Phys.* **1995**, *77*, 6588. (f) Kang, H.; Beauchamp, J. L. *J. Phys. Chem.* **1985**, *89*, 3364. (g) Cody, R. B.; Burnier, R. C.; Reents, W. D., Jr.; Carlin, T. J.; McCrery, D. A.; Lengel, R. K.; Freiser, B. S. *Int. J. Mass Spectrom. Ion Processes* **1980**, *33*, 37.

(18) (a) Szulejko, J. E.; McMahon, T. B. *Int. J. Mass Spectrom. Ion Processes* **1991**, *109*, 279. (b) Szulejko, J. E.; Fisher, J. J.; McMahon, T. B. *Int. J. Mass Spectrom. Ion Processes* **1988**, *83*, 147.

(19) Hiraoka, K.; Mizuse, S. *Chem. Phys.* **1987**, *118*, 457.

(20) (a) Claverie, P. In *Intermolecular Interactions*; Pullman, B., Ed.; John Wiley & Sons, Inc: New York, 1978; Chapter 2. (b) Brenner, V.; Zehnacker, A.; Lahmani, F.; Millie, P. *J. Phys. Chem.* **1993**, *97*, 10570. (c) Brenner, V. Thèse de l'Université de Paris-Sud, 1993. (d) Brenner, V.; Millie, P. *Z. Phys. D* **1994**, *30*, 327. (e) Liotard, D. *Int. J. Quantum Chem.* **1992**, *44*, 723.

(21) (a) Berthomieu, D.; Brenner, V.; Ohanessian, G.; Denhez, J.-P.; Millie, P.; Audier, H. E. *J. Am. Chem. Soc.* **1993**, *115*, 2505. (b) Berthomieu, D.; Brenner, V.; Ohanessian, G.; Denhez, J.-P.; Millie, P.; Audier, H. E. *J. Phys. Chem.* **1995**, *99*, 712.

(22) (a) Frisch, M. J.; Trucks, G. W.; Schlegel, H. B.; Gill, P. M.W.; Johnson, B. G.; Robb, M. A.; Cheeseman, J. R.; Keith, T.; Petersson, G. A.; Montgomery, J. A.; Raghavachari, K.; Al-Laham, M. A.; Zakrzewski, V. G.; Ortiz, J. V.; Foresman, J.B.; Cioslowski, J.; Stefanov, B. B.; Nanayakkara, A.; Challacombe, M.; Peng, C. Y.; Ayala, P. Y.; Chen, W.; Wong, M. W.; Andres, J. L.; Replogle, E. S.; Gomperts, R.; Martin, R.L.; Fox, D. J.; Binkley, J. S.; Defrees, D. J.; Baker, J.; Stewart, J. P.; Head-Gordon, M.; Gonzalez, C.; Pople, J. A. *Gaussian* 94, Revision C.3; Gaussian, Inc.: Pittsburgh, PA, 1995. (b) Davidson, E. R.; Feller, D. *Chem. Rev.* **1986**, *86*, 681.

(23) These values were obtained from the best D_e values quoted in ref 12a by subtracting an estimated 1.5 kcal mol^{-1} to account for ZPVE, thermal, and ΔPV corrections. The value of 1.5 kcal mol^{-1} is based on the computed values for CH_3CN and $(CH_3)_2O$ which are 1.2 and 1.5 kcal mol^{-1} as described herein.

(24) When an atomic ion clusters with a polyatomic neutral molecule, an entropy change, which is less negative than that normally found for polyatomic ions, is observed. This can be understood from the fact that the net entropy change is a result of the very significant loss in translational entropy, due to the loss of three translational degrees of freedom in proceeding from two particles to one, which is compensated for to a certain degree by the gain in rotational and vibrational entropy of the cluster relative to reactants. In the case of atomic reactants there are no rotational or vibrational degrees of freedom and thus, on a percentage basis, the gain in rotational entropy, due to the significant increase in moment(s) of inertia, is considerably greater. If the new vibrational modes of the cluster ion are of low frequency then a similar argument may apply to a relatively favorable gain in vibrational entropy as well.

(25) Dalleska, N. F.; Tjelta, B. L.; Armentrout, P. B. *J. Phys. Chem.* **1994**, *98*, 4191.